34th Annual International Conference of the IEEE EMBS
San Diego, California USA, 28 August - 1 September, 2012

On the Use of Smart Stents for Monitoring In-Stent Restenosis*

Kamyar Keikhosravy, Arash Zargaran-Yazd, and Shahriar Mirabbasi

Abstract— **In angioplasty with stent placement, re-narrowing of the artery within the stent site may occur due to the body's natural response to "heal" the stented area. This re-narrowing, also known as "in-stent restenosis", usually occurs within 6 months after surgery. To monitor and diagnose in-stent restenosis, passive telemonitoring using smart stents has been already proposed. In this paper, we present a feasibility study and advocate the use of an alternative method, namely active telemonitoring, which uses an integrated circuit embedded on the smart stent. Electromagnetic simulations and *in-vitro* measurements are presented to find the suitable range of frequency to wirelessly transfer power to the active device embedded on the smart stent. Furthermore, the range of induced power levels are simulated and experimentally verified.**

I. Introduction

Coronary angioplasty is a method commonly used to treat clogged coronary arteries and sometimes followed with the placement of a stent. A stent is a mesh-like tubular structure which holds open the narrowed section of the blood vessel. However, re-narrowing of the artery (in-stent restenosis) at the stented site may occur a few months after surgery (on average 6 months [1]) by the mechanism of thrombosis, i.e., clotting of the blood inside a blood vessel, and/or excessive tissue growth at the inner wall of vessel at the stented site (body's response to the external stent). Despite the successful reduction of re-narrowing by utilizing drug-eluted stents (DES), such stents only delay the re-narrowing process. A recent study on restenosis using different types of DES shows that the restenosis rate per stent is 3.5% after 1 year reaching to 4.9% after 2 years and that the risk of restenosis is higher in patients with diabetes mellitus [2]. Ongoing monitoring of in-stent restenosis is important and conventional monitoring approaches rely on imaging techniques which are either invasive such as angiography-based techniques [3] or non-invasive such as contrast-enhanced transthoracic echocardiography [4]. In either case, such techniques are typically costly and some level of patient discomfort is associated with such techniques. Therefore, many research and development activities have been focused on implementation of non-invasive and lower cost chronic monitoring systems for diagnosing restenosis. In particular, the use of wireless telemetry systems in conjunction with stents with embedded capacitive pressure sensors has attracted interest in recent years [5]–[12]. By tracking the blood pressure difference between the two ends of the stent the status of restenosis can be monitored. We refer to stents with embedded sensors as "smart stents". This idea has been studied in [5] to diagnose the restenosis in an aneurysm with an Endosure wireless pressure measurement device [8, 9] which has been implanted with the stent. However, due to the large size of such sensors they cannot be used in a coronary artery. A similar technique is used to monitor cardiovascular system stents with implantable sensory devices powered by implanted batteries [10]. However, this approach was a proof-of-concept and due to the large size of the battery using them in stents is not still quite practical and would increase the chance of restenosis.

To eliminate the need for a battery, a passive approach using an inductive stent has been presented in [13]. In this paper, the feasibility of an alternative approach with an improved sensitivity in monitoring the pressure difference is presented. In this technique, it is envisioned that a thinned integrated circuit (IC) with two on-chip oscillators is embedded on the stent structure. The oscillators will be powered wirelessly through the stent (acting as an inductor). The blood pressure on each side of the stent changes the capacitance of the corresponding embedded pressure sensor, which in turn change the transmitting frequency of the integrated capacitance to frequency converter (CFC) circuit. The CFC circuit transmits the signals using inductive stent presented in [14].

The structure of the paper is as follows: Section II presents the basic design and structure of the smart stent. This section also studies the electromagnetic properties and geometry of tissues located between the external monitoring device (the "reader") and the smart stent. Simulation results along with in-vitro experimental results are provided in Section III. Finally, Section IV provides concluding remarks.

II. Active Telemonitoring using Smart Stents

In the proposed telemetry approach, referred to as active (tele)monitoring technique, an IC whose substrate is thinned so that the thickness of the die is approximately 100 μm or lower will be embedded on designated small platform on the stent (refer to Fig. 2). The IC includes a CFC circuit consisting of an LC oscillator. The inductor (L) of CFC is integrated on-chip and the capacitance (C) is the capacitance of the pressure sensor capacitor. In this case, the stent acts as an inductor and has an important role in the overall system, i.e., it acts like an antenna both to receive power and send data to the external reader. Therefore, it is critical to find the suitable range of operation frequency for such wireless

*This work is supported in part by a Collaborative Health Research Project (CHRP) grant. Access to computer-aided-design (CAD) tools is facilitated by CMC Microsystems.

The authors are with the Department of Electrical and Computer Engineering, University of British Columbia, Vancouver, BC, V6T 1Z4, Canada ({keikhosr, arashz, shahriar}@ece.ubc.ca).

power and data transmission to improve the performance and reliability of the smart stent.

A. Optimum Frequency Range for Passive and Active Monitoring Techniques

Most of the reported inductively coupled bio-telemetry devices operate in sub-GHz frequencies [5, 8, 9, 13, 15] which is based on the fact that live tissues have more absorption for incident electromagnetic waves at higher frequencies. However, due to the sudden change of medium on the skin surface of the patient (air to skin interface) a portion of incident wave reflects from the surface of skin and as a result reduces the intensity of the signal penetrating into the body. Lower frequency signals experience more reflection. Thus, considering both absorption and reflection, there exist a frequency range over which the transmitted power gain is acceptable. A recent study [16] and measurement results [6, 7, 10] confirm that the attenuation of electromagnetic signals in tissue becomes significant at frequencies above 10 GHz. On the other hand, considering the size of the stent and its role as a receiver antenna, for frequencies lower than 0.1 GHz, the antenna loss becomes significant. Thus, one can expect that the optimum transmission frequency lies between 0.1 and 10 GHz (the lower limit depends on the size and structure of the stent which in this case acts dually as an antenna).

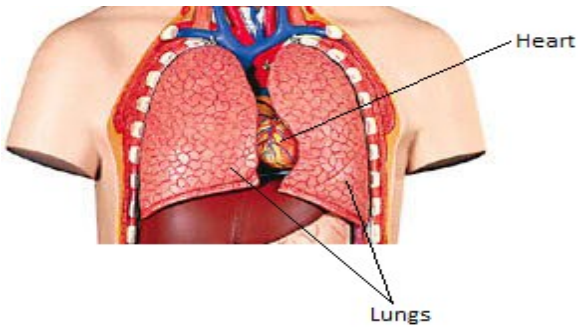

Fig. 1. Different layers of the torso. Note that the coronary arteries are not covered by lung (front view)

B. Modeling the Environment

In this study, we have used two popular electromagnetic 3-dimensional (3D) simulators, namely, Comsol Multiphysics® and ANSYS HFSS® (high-frequency structure simulator). First, we consider the geometry of the tissue surrounding the implanted smart stent. Fig. 1 shows a simplistic view of the layers of tissues in the human torso around the site of the coronary arteries where such stents are typically implanted. Note that the lungs do not cover the heart.

Table 1 lists different tissues between the outer surface of the epidermis (skin) and the coronary artery. These tissues and their average thickness are as follows: skin with 1.22 mm average thickness, adipose (fat) with 10 mm, Ribs with 20 to 25 mm, pericardium with 1.15 mm and finally coronary artery-wall with average thickness of 1.2 mm. The average distance between heart and exterior of the skin is around 39 mm [17].

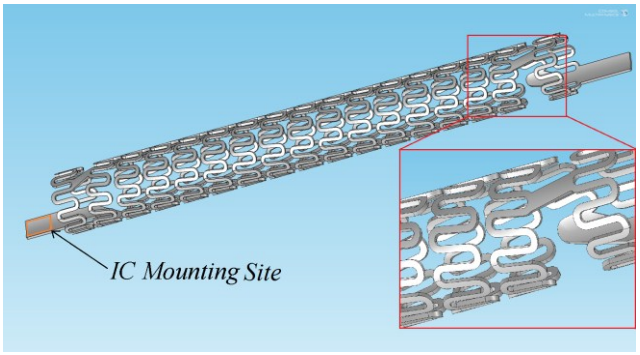

Fig. 2. 3D view of the antenna stent applied in this study

To model the tissues' absorption, the loss tangent of each type of tissue is calculated in different frequencies. In this study, the following equation for equivalent complex permittivity of tissues at a given frequency, i.e., $\hat{\varepsilon}(\omega)$, is used [18]:

$$\hat{\varepsilon}(\omega) = \varepsilon_\infty + \sum_{n=1}^{5} \frac{\Delta\varepsilon_n}{1 + (j\omega\tau_n)^{(1-\alpha_n)}} + \frac{\sigma_i}{j\omega\varepsilon_0}$$

where the magnitude of dispersion is described as $\Delta\varepsilon_n = \varepsilon_s - \varepsilon_\infty$, ε_∞ is the permittivity at field frequencies where $\omega\tau \gg 1$, ε_s is the permittivity at $\omega\tau \ll 1$, σ_i is the static ionic conductivity and ε_0 is the permittivity of free space, τ is time constant of polarization mechanism and ω is the angular frequency of the electric field. This model has been developed based on measured electric permittivity of different tissue types over the frequency ranging from 10 Hz to 100 GHz [18]. The values for permittivity of different tissues at different frequencies are extracted and summarized in Table 1 (j is the imaginary unit $j = \sqrt{-1}$). In this work the stent is made of stainless steel AISI 4340 which has a sheet resistance of $2.48 \times 10^{-7}\ \Omega m$.

TABLE I. RELATIVE PERMTIIVITY OF DIFFERENT TISSUES AT VARIOUS FREQUENCIES

Tissue	Thickness	Relative Permittivity (ε_r)			
		1 MHz	100MHz	1 GHz	3 GHz
Skin-Dry	1.22 mm	990.8 – *j*234.3	72.93 – *j*88.27	40.94 – *j*16.17	37.3 – *j*10.40
Adipose	10 mm	27.22 – *j*270	6.07 – *j*4.73	5.45 – *j*0.78	5.20 – *j*0.73
Rib	25 mm	144.5 – *j*437.7	15.28– *j*11.56	12.36 – *j*2.8	10.97 – *j*3.07
Peri-cardium	1.15 mm	1836 – *j*9036	65.97 – *j*127.2	54.81– *j*17.58	51.86 – *j*12.91
Blood Vessel	1.2 mm	3 – *j*1654	3 – *j*16.54	3 – *j*1.65	3 – *j*0.523
Blood	5 mm	3026 – *j*14777	76.81– *j*221.6	61.06 – *j*28.45	57.08 – *j*18.26

III. SIMULATION AND EXPERIMENTAL RESULTS

For the purpose of simulation, the external coil is assumed to have a distance of 4 mm from the skin surface, while the smart stent is oriented in parallel with skin surface as well as the external coil axis. The 3D view of the stent used in this simulation is shown in Fig. 2. The stent has a diameter of

1.7 mm and a length of 20 mm. For proper operation of embedded monitoring IC, a certain amount of power should be induced on the stent. The intensity of transferred power depends on the mutual coupling between the two coils (i.e., the external coil and the stent) and the magnitude of the excitation power of the external coil which is part of the monitoring device.

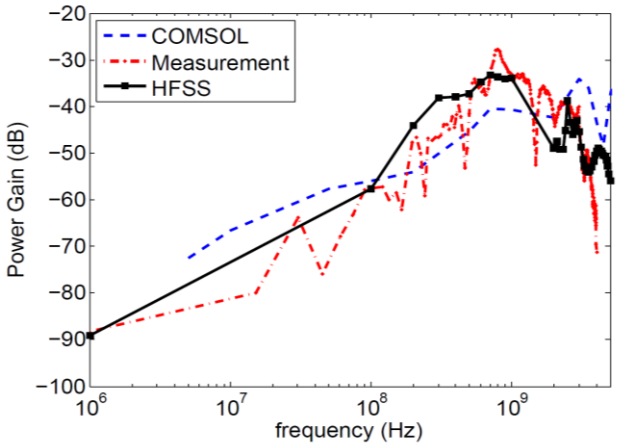

Fig. 3. Simulated and measured power gain for different excitation frequencies.

The value of the mutual coupling is proportional to the dimensions of the smart stent, and as explained earlier the amount of signal and thus the amount of power transferred to the stent is attenuated by the loss in different tissues within the body. The maximum excitation power at the external coil, set by the Federal Communication Council (FCC), limits the maximum radio-frequency radiation exposure (RRE) [19] to lower than 5 $\mathrm{mW/cm^2}$ over the frequency range of 0.1 to 5 GHz (For frequencies below 1500 MHz the power limit is frequency in MHz divided by 300).

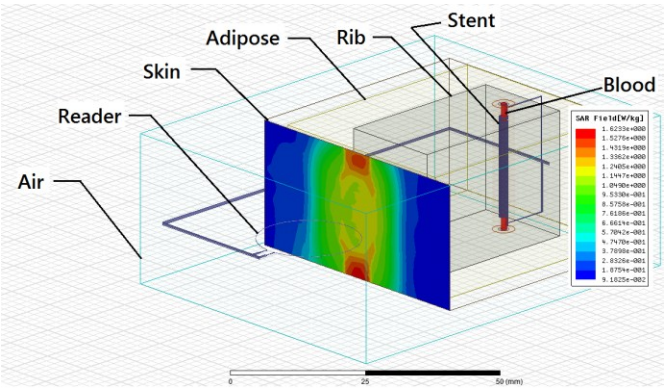

Fig. 4. Simulation setup in HFSS®. The 2D contour of specified absorption rate (SAR) is shown on the skin surface. This value is kept below the maximum allowable of 1.6 W/kg.

The simulation setup in HFSS® (and COMSOL®) is presented in Fig. 4. To increase the operational frequency of the external reader, a simple coil antenna is designed and modeled. Furthermore, the simulation results are compared with *in-vitro* measurement results. As expected (and as analyzed in [16]), there is an optimum frequency for power gain transmission for smart stent at which the power transmission gain reaches –28 dB. Fig. 3 shows that the optimum frequency for the smart stent of Fig. 2 is ~0.8 GHz. As shown in Fig. 5, by applying $P_{in} = 35.58$ mW, the maximum power density on the skin reaches to 2.56 $\mathrm{mW/cm^2}$ (which is very close to the maximum allowable of 2.66 $\mathrm{mW/cm^2}$ at 800 MHz). The maximum deliverable power to the stent will be:

$$P_L{}^{max} = G_p{}^{max} \cdot P_{in} \qquad (1)$$

where $G_p{}^{max}$ is the maximum operating power gain of the system and P_{in} is the input power applied to the reader. As shown in Fig. 3 the maximum operating power gain is located around 0.8 GHz and is approximately equal to –28 dB (confirmed by measurement). By plugging this value into (1), the maximum deliverable power to the stent (with 50 ohm terminations on both sides) is about 56 µW at 800 MHz.

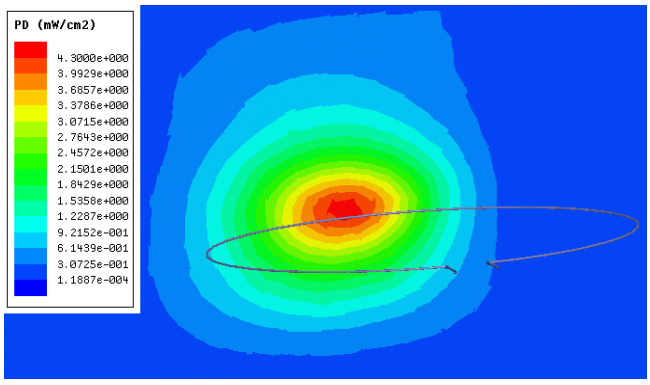

Fig. 5. Power density (PD) of the excitation signal, generated by reader on the surface of the skin (at 2 GHz).

Assuming that most of the transferred power will be used for the transmission of sensor signals (in this case, 50 µW), we can calculate the power density of the backward link established by internal IC on the surface of the skin. Fig. 6 presents the 2D map of observable power density on the skin surface, transmitted from the smart stent. The power density reaches to around 5 $\mathrm{pW/cm^2}$ in the vicinity of the skin surface (assuming that the stent is implanted at the depth 39 mm). These simulation results (Fig. 6) provides useful information for the design of the reader antenna.

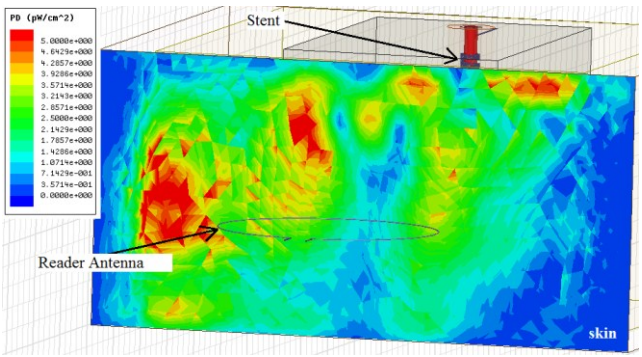

Fig. 6. Power density (PD) of signals transmitted by the stent.

To obtain the experimental results, the *in-vitro* setup similar to the simulation model has been used. To mimic the surrounding tissues around the implanted stent, the inductive stent is surrounded by ground beef with extra fat. The reader coil is the same as that modeled for EM simulations and is connected to one port of a vector network analyzer (VNA), Anritsu MS2034A. The two sides of the stent are connected to the other port of the VNA and the scattering parameters of the system are measured. The operating power gain is given by:

$$G_P = \frac{P_L}{P_{in}} = \frac{|S_{21}|^2(1-|\Gamma_L|^2)}{|1-S_{22}\Gamma_L|^2(1-|\Gamma_{in}|^2)} \quad (2)$$

where S_{21} and S_{12} are the forward and reverse gain scattering parameters of the system and Γ_L and Γ_{in} are the load and input reflection coefficients. P_L is the delivered power on the stent site and P_{in} is the excitation power at the reader terminal. Note that in this measurement (and simulation) setup, all system terminals are terminated to a 50 Ω impedance and therefore, $\Gamma_L = \Gamma_{in} = 0$. In such conditions, Eq. (2) for operating power gain (G_P) can be simplified to $G_P = |S_{21}|^2$. In this experiment, the stent has been surrounded by ground beef of the depth of 39 mm and the reader is located at 4 mm distance from the ground beef surface.

IV. Conclusion

In this work, the feasibility of using active wireless telemetry for monitoring in-stent restenosis in smart stents implanted in the coronary artery is investigated. The overall system is simulated using both HFSS® and COMSOL® Multiphysics and *in-vitro* experiments are conducted using a reader antenna and a stent that is surrounded by ground beef. The results obtained from simulation and measurement are in good agreement and show that a power of 56 μW at around 0.8 GHz frequency can be delivered to the stent which is a sufficient power to operate an IC embedded on the smart stent for active monitoring of in-stent restenosis. Furthermore, simulations studies show that the smart stent can use the abovementioned received power to transmit information with the power density level that reaches to around $5\,\mathrm{pW/cm^2}$ in the vicinity of the skin surface (assuming that stent is implanted at the depth of 39 mm). This information can be retrieved by a properly designed reader.

Acknowledgments

The authors would like to thank Lei Qin, Men Wang, Charles Lo, and Vibhav Agarwal for their help with COMSOL® simulations, Dr. Reza Rashidi for his assistance in developing the 3D model of the smart stent, Roozbeh Mehrabadi for computer-aided design (CAD) tools support, and Dr. Roberto Rosales for his technical assistance with measurements.

References

[1] P.W. Serruys H.E. Luijten, K.J. Beatt, et al., "Incidence of restenosis after successful coronary angioplasty: a time-related phenomenon: a quantitative angiographic study in 342 consecutive patients at 1, 2, 3, and 4 months," *Circulation.* 1988; 77: 361–371.

[2] O. Frobert, B. Lagerqvist, J. Carlsson, J. Lindback, U. Stenestrand, and S. K. James,"Differences in restenosis rate with different drug-eluting stents in patients with and without diabetes mellitus: A report from the scaar (swedish angiography and angioplasty registry)," *J Am Coll Cardiol*, vol. 53, no. 18, pp. 1660_1667, 2009. [Online] Available at: http://content.onlinejacc.org/cgi/content/abstract/53/18/1660, accessed on June 4, 2012.

[3] D. Oncel, G. Oncel, and M. Karaca, "Coronary stent patency and in-stent restenosis: Determination with 64-section multidetector CT coronary angiography—Initial experience," *Radiology*, vol. 242, no. 2, pp. 403-409, February 2007. [Online] Available at: http://radiology.rsna.org/content/242/2/403.full, accessed on June 4, 2012.

[4] M. Ruscazio, R. Montisci, P. Colonna, et al. "Detection of coronary restenosis after coronary angioplasty by contrast-enhanced transthoracic echocardiographic Doppler assessment of coronary flow velocity reserve," *Journal of the Amierican College of Cardiology*, vol. 40, no. 5, pp. 896-903, May 2002.

[5] J. Mazeyrat, O. Romain, P. Garda, E. Flecher, M. Karouia, P. Leprince, P.-Y. Lagree, and M. Destrade, "Wireless communicative stent for follow-up of abdominal aortic aneurysm," *IEEE Biomedical Circuits and Systems Conference (BioCAS)*, pp. 237-240, Nov. 29-Dec. 1, 2006.

[6] E.Y. Chow, A.L. Chlebowski, S. Chakraborty, W.J. Chappell, P.P. Irazoqui, "Fully Wireless Implantable Cardiovascular Pressure Monitor Integrated with a Medical Stent," *IEEE Transactions on Biomedical Engineering*, vol. 57, no. 6, pp. 1487-1496, June 2010.

[7] E.Y. Chow, Y. Ouyang, B. Beier, W.J. Chappell, and P.P. Irazoqui, "Evaluation of Cardiovascular Stents as Antennas for Implantable Wireless Applications," *IEEE Transactions on Microwave Theory and Techniques,* vol. 57, no. 10, pp. 2523-2532, Oct. 2009.

[8] M. Allen, M. Fonseca, J. White, Implantable wireless sensor for blood pressure measurement within an artery, WO Patent n°2004014456

[9] M. Allen, M. Fonseca, and J. White, Implantable wireless sensor, WO Patent n°03/061504 A1.

[10] E.Y. Chow, B. Beier, Y. Ouyang; W.J. Chappell, and P.P. Irazoqui, "High frequency transcutaneous transmission using stents configured as a dipole radiator for cardiovascular implantable devices," *IEEE MTT-S International Microwave Symposium*, pp. 1317-1320, June 2009.

[11] Denisov, A., Yeatman, E. , "Ultrasonic vs. Inductive Power Delivery for Miniature Biomedical Implants," *International Conference on Body Sensor Networks (BSN),* pp. 84-89, June 2010.

[12] A.D. DeHennis and K.D. Wise, "A fully integrated multisite pressure sensor for wireless arterial flow characterization," *Journal of Microelectromechanical Systems*, vol. 15, no. 3, pp. 678-685, June 2006.

[13] K. Takahata, Y.B. Gianchandani, and K.D. Wise, "Micromachined Antenna Stents and Cuffs for Monitoring Intraluminal Pressure and Flow," *Journal of Microelectromechanical Systems,* vol. 15, no. 5, pp.1289-1298, Oct. 2006.

[14] K. Takahata, A. DeHennis, K.D. Wise, and Y.B Gianchandani, "Stentenna: a micromachined antenna stent for wireless monitoring of implantable microsensors," *Int'l Conference of the IEEE Engineering in Medicine and Biology Society*, vol. 4, pp. 3360-3363, Sept. 2003.

[15] P. Vaillancourt, A. Djemouai, J.F. Harvey, and M. Sawan, "EM radiation behavior upon biological tissues in a radio-frequency power transfer link for a cortical visual implant," *International Conference of the IEEE Engineering in Medicine and Biology Society,* vol. 6, pp. 2499-2502, 30 Oct- 2 Nov, 1997.

[16] A. S. Y. Poon, S. O'Driscoll, and T. H. Meng, "*Optimal frequency for wireless power transmission into dispersive tissue,*" IEEE Trans. Antennas and Propagation, vol. 58, no. 5, pp. 1739–1749, May 2010.

[17] P.S. Rahko, "Evaluation of the skin-to-heart distance in the standing adult by two-dimensional echocardiography," Journal of the American Society of Echocardiography, vol. 21, no. 6, pp. 761-764, 2008. [Online]. Available: http://www.sciencedirect.com/science/article/pii/S0894731707007560, accessed on June 4, 2012.

[18] S. Gabriel, R. W. Lau and C. Gabriel," *The dielectric properties of biological tissues: III. Parametric models for the dielectric spectrum of tissues*", 1996 Phys. Med. Biol. 41 2271.

[19] Code of Federal Regulations (CFR) 47 FCC § 1.1310, "Radiofrequency Radiation Exposure Limits," 2011.